## Measurement-Induced Power-Law Negativity in an Open Monitored Quantum Circuit

Zack Weinstein<sup>®</sup>, <sup>1,\*</sup> Yimu Bao<sup>®</sup>, <sup>1</sup> and Ehud Altman<sup>1,2</sup>

<sup>1</sup>Department of Physics, University of California, Berkeley, California 94720, USA

<sup>2</sup>Materials Sciences Division, Lawrence Berkeley National Laboratory, Berkeley, California 94720, USA

(Received 22 February 2022; accepted 21 July 2022; published 19 August 2022)

Generic many-body systems coupled to an environment lose their quantum entanglement due to decoherence and evolve to a mixed state with only classical correlations. Here, we show that measurements can stabilize quantum entanglement within open quantum systems. Specifically, in random unitary circuits with dephasing at the boundary, we find both numerically and analytically that projective measurements performed at a small nonvanishing rate result in a steady state with an  $L^{1/3}$  power-law scaling entanglement negativity within the system. Using an analytical mapping to a statistical mechanics model of directed polymers in a random environment, we show that the power-law negativity scaling can be understood as Kardar-Parisi-Zhang fluctuations due to the random measurement locations. Further increasing the measurement rate leads to a phase transition into an area-law negativity phase, which is of the same universality as the entanglement transition in monitored random circuits without decoherence.

DOI: 10.1103/PhysRevLett.129.080501

The dynamics of quantum entanglement is being investigated extensively as a potential resource for quantum information processing [1–9]. Recent theoretical developments have shown that large-scale quantum entanglement can be established in monitored quantum systems undergoing unitary evolution interspersed by measurements [4,5,10–15]. For moderate measurement rates below a threshold, the entanglement generated by the unitary evolution can overcome the disentangling effect of measurements, leading to volume-law scaling of the entanglement entropy in individual quantum state trajectories at late times. Increasing the measurement rate beyond a critical value drives a measurement-induced phase transition (MIPT) to a steady state with area-law scaling of the entanglement entropy [4,5].

Studies of monitored systems thus far have largely focused on dynamics involving only unitary gates and projective measurements, which preserves the purity of the quantum state. Insofar as such monitored circuits can be understood as models for entanglement dynamics in generic many-body systems, they are missing an important ingredient. Real systems always exhibit unintended decoherent interactions with their environment, leading inevitably to mixed-state dynamics. Such effects typically destroy internal entanglement, as the system degrees of freedom become entangled with the infinite bath instead of with each other. For example, in monitored random circuits, a nonvanishing rate of decoherence throughout the bulk inevitably results in a short-range entangled steady state at late times [16]. It is therefore natural to ask if a monitored system with weaker decoherence can sustain large-scale entanglement in the steady state.

In this Letter, we address this question in models of onedimensional quantum circuits consisting of random unitary gates and measurements, coupled to an infinite bath at the boundary implemented as a dephasing quantum channel [see Fig. 1(a)]. Using the logarithmic entanglement negativity as a measure of mixed-state entanglement [17–26], we employ both numerical simulations of Clifford circuits and an analytical mapping to a statistical mechanics model to assess the scaling of internal entanglement in the circuit qubits.

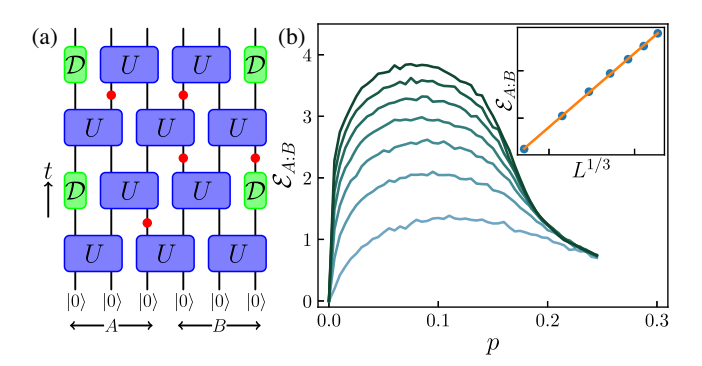


FIG. 1. (a) Circuit diagram for the model studied. Qudits are evolved under random unitary gates (blue) and projective measurements (red dots) occurring randomly at a rate p, along with dephasing channels (green) applied on the first and last qudit between each layer of unitary gates. (b) Late-time logarithmic negativity between subsystems A and B, taken to be the left and right halves of the qubit chain, as a function of measurement rate p. Different curves indicate various system sizes L, ranging from 40 (light blue) to 280 (dark green). Inset: Logarithmic negativity as a function of  $L^{1/3}$  (blue dots) at p=0.1, along with the fitting curve  $y=c_1L^{1/3}+c_2$  (orange line) with  $c_1\approx 0.779$  and  $c_2\approx -1.307$ . The numerical results are averaged over 200 random circuit realizations.

While the entanglement negativity vanishes in the absence of measurements as expected, we find numerically that the half-system negativity exhibits an  $L^{1/3}$  power-law scaling with system size for nonzero measurement rates below the MIPT critical point [see Fig. 1(b)]. This power law persists until a critical measurement rate  $p_c$ , above which the negativity exhibits an area law.

To develop a theoretical understanding of the observed power-law negativity, we build on previous works mapping the dynamics of entanglement entropy in random circuits to effective statistical mechanics models [3,16,27–29]. Using a similar replica formalism to previous works, we show that the negativity can be calculated using the same effective model of ferromagnetic spins with different boundary conditions [30]. The vanishing of the volume-law contribution to the negativity in the presence of dephasing channels is immediately seen to be a consequence of symmetry-breaking boundary conditions imposed by dephasing.

The exponent 1/3 has previously been observed in subleading contributions to the bipartite entanglement entropy in the pure state dynamics of circuit models, both in  $t^{1/3}$  subleading growth of entanglement entropy over time in pure unitary circuits [3,28], and in  $\ell^{1/3}$  subleading scaling of late-time entanglement entropy with subsystem size in monitored circuits within the volume-law phase [31]. This exponent was explained as the Kardar-Parisi-Zhang (KPZ) fluctuations of the domain walls, interpreted as directed polymers in a random environment [32–35]. Here, we analytically derive a mapping relating the negativity to a collection of directed polymers within a limit of large qudit dimension  $d \to \infty$  and verify its prediction of  $L^{1/3}$  negativity scaling. Building on previous works [28,31,36], we explicitly demonstrate the role of measurements in generating a random attractive potential on the polymers, which naturally lead to KPZ fluctuations in the negativity for nonzero measurement rates.

Model.—We consider a chain of L d-qudits with open boundary conditions, initialized in the product state  $|0\rangle^{\otimes L}$ , and evolved under a brick-wall random unitary circuit [see Fig. 1(a)], where each gate is independently drawn from the Haar ensemble. In between layers of unitary gates, each ith qudit is measured in the computational basis  $\{|a\rangle\}_{a=0}^{d-1}$  with probability p, which collapses the system onto the state  $\rho\mapsto P_i^a\rho P_i^a/\mathrm{tr}(P_i^a\rho)$  with probability  $\mathrm{tr}(P_i^a\rho)$  given by the Born rule, where  $P_i^a=|a\rangle\langle a|_i$  projects the ith qudit onto the state  $|a\rangle$ . To model the coupling to an infinite bath, the boundary qudits i=1 and i=L are subjected to local dephasing described by  $\mathcal{D}_i[\rho]=\sum_{a=0}^{d-1}P_i^a\rho P_i^a$  [37,38]. This coupling can also be understood as a measurement in which we average the density matrix over all possible measurement outcomes.

The addition of dephasing channels results in opensystem dynamics and inevitably drives the system into a mixed state, for which the von Neumann entropy is no longer a meaningful measure of entanglement [39,40]. To quantify quantum entanglement within the system at late times, we employ the logarithmic negativity [18–26,30], a measure of mixed-state bipartite entanglement and a rigorous upper bound to the distillable entanglement of a mixed state [17,40–44]:

$$\mathcal{E}_{A \cdot B}[\rho] = \log \|\rho^{T_B}\|_1,\tag{1}$$

where  $\rho^{T_B}$  is the partial transpose of  $\rho$  in subsystem B, and  $\|\cdot\|_1$  denotes the trace norm. Throughout this Letter, we take A and B to respectively consist of the left and right halves of the qudit chain. Note that Ref. [25] previously used the logarithmic negativity to characterize the conformal field theory underlying the MIPT without decoherence.

Numerical results.—To efficiently simulate the circuit, we employ random Clifford unitary gates acting on d=2 qubits using the stabilizer formalism [3,10,45–49]. While the Clifford gates are not generic, they form a unitary 3-design [50] and are expected to give the same qualitative behavior as the Haar random circuit. The late-time negativity as a function of measurement rate p for system sizes up to L=280 is shown in Fig. 1(b).

In the case without measurements (i.e., p=0), the latetime negativity is uniformly zero independent of system size. This is to be expected both from general physical considerations and from Page's theorem [24,51,52]: if the dephasing channels are understood as an effective coupling to an infinitely large bath, then the system becomes maximally entangled with the bath at late times and no bipartite entanglement within the system remains.

Remarkably, the negativity sharply increases as p increases from zero and exhibits nontrivial scaling with the system size. At moderate measurement rates, for example p=0.1, the scaling of the negativity is consistent with a power law of the form  $\mathcal{E}_{A:B}=c_1L^{1/3}+c_2$  for two fitting parameters  $c_{1,2}$  as shown in the inset.

At sufficiently high measurement rates, the negativity begins to decrease as a function of measurement strength. This culminates in a measurement-induced transition at  $p_c$  in which the power-law coefficient  $c_1$  vanishes. Since our circuit model differs from previous pure-state circuits only in its boundary conditions, we expect the bulk critical behavior to be identical to that of the ordinary MIPT without dephasing. In the Supplemental Material [49] we perform a finite-size scaling analysis and find  $p_c \simeq 0.16$  consistent with previous works [4,10,53], but we cannot reliably extract a correlation length exponent  $\nu$  due to the numerical smallness of the negativity.

Effective statistical mechanics model.—Our numerical results can be understood analytically by relating the averaged logarithmic negativity to the free energy of directed polymers in a random environment. Here, we consider the Haar random circuit acting on d-qudits with

 $d \to \infty$  allowing for greater analytical control [3,16,28,29,49]. Within the effective model, the  $L^{1/3}$  negativity scaling can be understood as KPZ fluctuations of the directed polymers. Complete details of the statistical mechanics model can be found in the Supplemental Material [49].

The *n*th Rényi negativity [19–22] (properly defined for  $n \ge 4$ ) for a *fixed* set of measurement locations **X** in spacetime, averaged over Haar unitary gates  $\mathcal{U} = \{U_{ij,t}\}$  and measurement outcomes **m**, is given by

$$\overline{\mathcal{E}_{A:B}^{(n)}(\mathbf{X})} = \mathbb{E}_{\mathcal{U}} \sum_{\mathbf{m}} p_{\mathbf{m}} \frac{1}{2-n} \log \left\{ \frac{\operatorname{tr}[(\rho_{\mathbf{m}}^{T_B})^n]}{\operatorname{tr}\rho_{\mathbf{m}}^n} \right\}, \quad (2)$$

where  $\rho_{\mathbf{m}}$  is the unnormalized density matrix obtained along the measurement trajectory  $\mathbf{m}$ , and  $p_{\mathbf{m}} = \mathrm{tr} \rho_{\mathbf{m}}$  is the probability for achieving the measurement outcomes  $\mathbf{m}$  conditioned on the locations of the measurements  $\mathbf{X}$  and the unitary realization  $\mathcal{U}$ . The logarithmic negativity [Eq. (1)] is obtained from Eq. (2) using the peculiar limit  $n \to 1$  along even n [19,20].

To facilitate the mapping, we employ the replica trick [35,54] to write  $\overline{\mathcal{E}_{A:B}^{(n)}} = \lim_{k\to 0} \mathcal{E}_{A:B}^{(n,k)}$ , where  $\mathcal{E}_{A:B}^{(n,k)}$  can be interpreted as being proportional to the difference of two free energies:

$$\mathcal{E}_{A:B}^{(n,k)}(\mathbf{X}) = -\frac{1}{k(n-2)} \log \left\{ \frac{Z^{(n,k)}}{Z_0^{(n,k)}} \right\},\tag{3}$$

where the two "partition functions"  $Z^{(n,k)}$  and  $Z_0^{(n,k)}$  differ only in their boundary conditions at the final time slice. Note that these partition functions contain the averages over unitary realizations and measurement outcomes, but *not* the locations of measurements; following Ref. [36], and in contrast to previous works [16,29], we leave the locations of measurements as quenched disorder.

As in previous works [16,28,29,36,55–58], averaging over Haar random unitary gates results in a sum over pairing configurations between the replicated copies of the density matrix. The bulk effective statistical mechanics model is then a lattice magnet containing permutationvalued spins with ferromagnetic interactions, where a given permutation  $\sigma$  from the permutation group  $S_{nk+1}$  represents a local tensor contraction between each  $\ell$ th ket and the  $\sigma(\mathscr{E})$ th bra. The boundary conditions of  $Z^{(n,k)}$  and  $Z_0^{(n,k)}$  at the final time, which are unique to the calculation of the Rényi negativity [30], are shown in Fig. 2:  $Z^{(n,k)}$  contains cyclic permutations  $\mathbb{C}$  at the top of region A and anticyclic permutations  $\bar{\mathbb{C}}$  at the top of region B, while  $Z_0^{(n,k)}$  contains cyclic permutations along the entire top boundary.  $\mathcal{E}_{A:B}^{(n,k)}$  is thus proportional to the free energy cost of imposing a domain wall between  $\mathbb{C}$  and  $\overline{\mathbb{C}}$  at the interface of A and B at the final time boundary. In the analytically tractable  $d \to \infty$ 

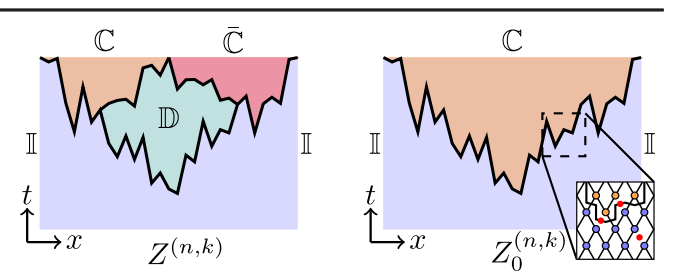


FIG. 2. Schematic zero temperature spin configurations of  $Z^{(n,k)}$  and  $Z_0^{(n,k)}$  for a fixed disorder realization of measurement locations. The final time boundary conditions are shown at the top of each diagram:  $Z^{(n,k)}$  contains cyclic permutations  $\mathbb C$  (orange) at the top of region A and anticyclic permutations  $\mathbb C$  (red) at the top of region B, while  $Z_0^{(n,k)}$  contains cyclic permutations along the entire top boundary. Dephasing at the left and right boundaries of the chain enforces identity permutations  $\mathbb I$  (blue) at the left and right boundaries of the effective model. An intermediate domain of spins  $\mathbb D$  (green) appears in  $Z^{(n,k)}$  by a similar mechanism as in Ref. [30]. Viewing domain walls as collections of polymers, measurements result in a random attractive potential on the polymers, leading to KPZ fluctuations in the negativity.

limit, the energetic cost per length of a domain wall away from a measured site is [16,28,29]

$$\beta E(\sigma_i, \sigma_j) = |\sigma_i^{-1} \sigma_j| \log d \qquad (d \to \infty),$$
 (4)

where  $|\sigma_i^{-1}\sigma_j|$  is the number of transpositions required to obtain the permutation  $\sigma_j$  from  $\sigma_i$ . The limit  $d \to \infty$  imposes zero temperature,  $\beta^{-1} \to 0$ . Reference [28] argued (in the absence of measurements) that a domain wall between permutations  $\sigma_i$  and  $\sigma_j$  should be viewed as a collection of  $|\sigma_i^{-1}\sigma_j|$  "elementary" domain walls given by transpositions, which become noninteracting in the  $d \to \infty$  limit according to Eq. (4). Weak interactions between such elementary domain walls can be calculated perturbatively in powers of 1/d.

The presence of boundary dephasing channels modifies the left and right boundary conditions of the effective model. In contrast to the open boundary conditions for models without decoherence [28], dephasing imposes identity permutation spins  $\mathbb{I}$  at the left and right boundaries, leading to the domain wall structure in Fig. 2; note that an intermediate domain of spins  $\mathbb{D}$  (green) can appear in  $Z^{(n,k)}$  without additional energy cost provided that  $|\sigma^{-1}\mathbb{D}|+|\mathbb{D}^{-1}\tau|=|\sigma^{-1}\tau|$  for  $\sigma,\tau=\mathbb{C},\bar{\mathbb{C}},\mathbb{I}$  [30,49]. Using Eq. (4), this domain wall structure leads to a negativity in the  $d\to\infty$  limit of the form

$$\mathcal{E}_{A:B}^{(n,k)}(\mathbf{X}) = \frac{\log d}{2} \{ \ell_A + \ell_B - \ell_{AB} \},\tag{5}$$

where  $\ell_R$  is the length of the minimal domain wall separating the top boundary of region R from the rest of

the system. Note that this quantity is independent of the replica indices (n,k), allowing for the replica limit to be trivially taken. In the absence of measurements these domain walls take straight lines through the system, and the negativity therefore vanishes [49]. This is consistent both with the expectation from Page's theorem and the p=0 numerical results of Fig. 1.

To explain the  $L^{1/3}$  scaling of negativity at nonzero measurement rates, we must address the role of measurements in the effective spin model. By keeping the spacetime locations of measurements as unaveraged quenched disorder, we find that measurements effectively eliminate the ferromagnetic bonds between adjacent spins. In the  $d \to \infty$  limit, each domain wall will optimize to pass through as many measurement locations as possible to minimize its energy. Viewing each domain wall as a collection of polymers as in [28], the elimination of ferromagnetic bonds can be understood as a random attractive potential on the polymers, wherein the energy of a polymer is reduced by  $\log d$  for each measured site the polymer passes through. The total energy cost of a single polymer, directed [59] in the x direction with spatial profile y(x), is given by

$$\beta H[y(x)] = \log d \int dx \left\{ 1 + \frac{1}{2} (\partial_x y)^2 + V(x, y) \right\}, \quad (6)$$

where V(x,y) is a random potential with mean  $p \log d$  and variance  $p(1-p)(\log d)^2\delta(x-x')\delta(y-y')$ .  $\mathcal{E}_{A:B}^{(n,k)}$  is then simply proportional to the sum of the polymer ground state energies in  $Z^{(n,k)}$ , minus those in  $Z^{(n,k)}_0$ . Each such energy may then be averaged over measurement locations independently.

The free energy of a directed polymer in a random environment has been well-studied—it is equivalent to the KPZ equation via the Hopf-Cole transformation [32,33,35,60]. Since the polymers here are restricted to the half-plane below the final time slice, a solution for the free energy of each polymer is obtained from the KPZ equation in the half-plane, which can be calculated analytically using Bethe ansatz methods [31,61,62]. The result is an energetic contribution  $s_0\ell + s_1\ell^{1/3}$  for each polymer of horizontal length  $\ell$ , where  $s_0$  and  $s_1$  are nonuniversal positive constants. It can then be seen from Eq. (5) that the linear contributions from each polymer cancel as in the p=0 case, but the  $\ell^{1/3}$  contributions due to KPZ fluctuations in the polymer lengths do not-they yield a positive  $L^{1/3}$  growth of the averaged Rényi negativity  $\overline{\mathcal{E}_{A:B}^{(n)}}$ . Although this analytical argument cannot compute the dependence of the power-law coefficient  $s_1$  on the measurement rate, the qualitative prediction of  $L^{1/3}$  negativity scaling for nonzero measurement rates is consistent with the Clifford numerical results.

Discussion.—We have shown that the active monitoring of a random quantum circuit with decoherence at the

boundaries can stabilize large-scale entanglement. This is evinced by the  $L^{1/3}$  power-law scaling of late-time entanglement negativity, which is obtained only for nonzero measurement rates below a critical threshold  $p_c$ . The enhancement of quantum entanglement by measurements in the presence of decoherence stands in contrast with the effect of measurements in random circuits featuring strictly pure-state dynamics [4,5,10,11,16,29], wherein measurements disentangle system qubits from each other and decrease the internal entanglement of the system. Here, in the mixed-state dynamics, measurements can play an additional role by curtailing decoherence. This occurs both by disentangling system qudits from the bath, allowing them to reentangle with each other, as well as by diminishing long-range entanglement structures with which the boundary dephasing channels could decohere the bulk. Remarkably, while measurements cannot protect the full volume-law entanglement from decoherence, the interplay between dephasing and measurements has revealed the "critical"  $L^{1/3}$  scaling of entanglement that was previously hidden as a subleading contribution in the pure-state dynamics [31].

In random Clifford circuits with strictly pure-state dynamics, the distribution of stabilizer lengths has previously offered insight on the bipartite entanglement entropy [10]. It is therefore interesting to see how the stabilizer length distribution is modified in the presence of boundary dephasing channels (see Fig. 3). Although the length distribution does not directly determine the negativity in a mixed state, it can be used to compute the mutual information  $I_{A:B} = S_A + S_B - S_{AB}$  [37], which shows qualitatively similar behavior to the negativity [49] despite failing as a mixed-state entanglement measure. On one hand, we see that dephasing channels act as a stabilizer "sink" by destroying the buildup at lengths

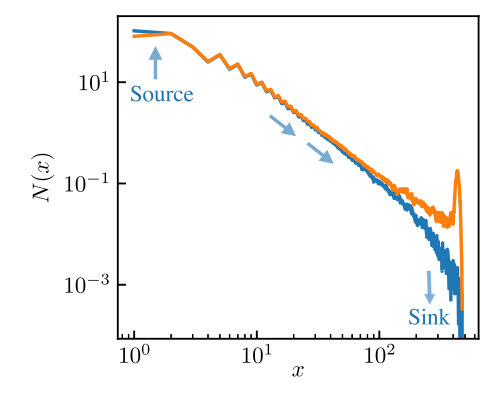


FIG. 3. Late-time stabilizer length distribution in log-log scale. Here, we consider a circuit with decoherence at two random sites rather than two edges in each time step. Blue and red curve represent the results with and without dephasing baths at the boundary, respectively. The numerical simulation is performed in the circuits of size L=480 and with measurement rate p=0.1. The results are averaged over 200 random circuit realizations.

x = L/2, which was previously responsible for the volume-law contribution to the mutual information with no dephasing [10]. On the other hand, measurements can act as a "source," both by creating new short stabilizers, and by preventing stabilizers from becoming so long that they reach the system boundaries and dephase. This is evident in the power-law ramp, which is robust to dephasing and would be absent without measurements, and is responsible for the power-law scaling of  $I_{A:B}$ . The resulting steady-state dynamics of the stabilizer length distribution is reminiscent of energy transfer under turbulent cascade, and it is tempting to develop an effective classical model for the stabilizer dynamics to capture the power law length distribution.

It is also interesting to consider how the negativity is affected by replacing the Markovian quantum channels with explicit bath qudits. For bath sizes smaller than the system, it is expected by Page's theorem that the negativity within the system can retain volume-law scaling in the absence of measurements. However, since the continuous monitoring of the system reduces the effective number of qudits participating in the system-bath entanglement dynamics, the negativity can undergo a first order Pagelike transition within the volume-law entropy phase of the monitored circuit. The details of this Page-like negativity transition will be left for future work [63].

In our analysis, it was crucial that decoherence occurred only at the boundary. Instead, bulk decoherence will manifest as a symmetry-breaking field in the statistical mechanics model reducing  $(S_{nk+1} \times S_{nk+1}) \rtimes \mathbb{Z}_2$  down to a residual  $S_{nk+1} \times \mathbb{Z}_2$  symmetry [64]. The decoherence pins the spins to the state I, which is symmetric under the residual symmetry, resulting in a maximally mixed state in the circuit. To establish a large-scale entanglement negativity in the presence of bulk decoherence, one needs to spontaneously break the residual  $\mathbb{Z}_2$  Hermiticity symmetry. One possibility is to introduce additional nonunitary elements, such as active feedback. A designed feedback process using the knowledge of measurement results might possibly create preference of  $\mathbb{C}$  and  $\mathbb{C}$  over  $\mathbb{I}$ , leading to a residual  $\mathbb{Z}_2$  symmetry-breaking state with large-scale entanglement.

More broadly, we expect our results to be relevant beyond random circuit models to more realistic Hamiltonian dynamics. Given the significant recent interest in open-system quantum dynamics, it is interesting to consider whether the unique interplay between measurements and decoherence exhibited here can lead to new phases of nonequilibrium dynamics in settings accessible to modern experiments.

We thank Soonwon Choi, Zala Lenarčič, and Yaodong Li for useful discussions. This work was supported in part by the NSF QLCI program through grant no. OMA-2016245. Z. W. is supported by the Berkeley Connect fellowship.

- zackmweinstein@berkeley.edu
- [1] H. Kim and D. A. Huse, Phys. Rev. Lett. **111**, 127205 (2013).
- [2] A. M. Kaufman, M. E. Tai, A. Lukin, M. Rispoli, R. Schittko, P. M. Preiss, and M. Greiner, Science 353, 794 (2016).
- [3] A. Nahum, J. Ruhman, S. Vijay, and J. Haah, Phys. Rev. X 7, 031016 (2017).
- [4] Y. Li, X. Chen, and M. P. A. Fisher, Phys. Rev. B 98, 205136 (2018).
- [5] B. Skinner, J. Ruhman, and A. Nahum, Phys. Rev. X 9, 031009 (2019).
- [6] F. Arute, K. Arya, R. Babbush, D. Bacon, J. C. Bardin, R. Barends, R. Biswas, S. Boixo, F. G. Brandao, D. A. Buell et al., Nature (London) 574, 505 (2019).
- [7] J. Choi, A. L. Shaw, I. S. Madjarov, X. Xie, J. P. Covey, J. S. Cotler, D. K. Mark, H.-Y. Huang, A. Kale, H. Pichler et al., arXiv:2103.03535.
- [8] C. Noel, P. Niroula, A. Risinger, L. Egan, D. Biswas, M. Cetina, A. V. Gorshkov, M. Gullans, D. A. Huse, and C. Monroe, Nat. Phys. 18, 760 (2022).
- [9] M. Ippoliti, M. J. Gullans, S. Gopalakrishnan, D. A. Huse, and V. Khemani, Phys. Rev. X 11, 011030 (2021).
- [10] Y. Li, X. Chen, and M. P. A. Fisher, Phys. Rev. B 100, 134306 (2019).
- [11] S. Choi, Y. Bao, X.-L. Qi, and E. Altman, Phys. Rev. Lett. 125, 030505 (2020).
- [12] M. J. Gullans and D. A. Huse, Phys. Rev. X 10, 041020 (2020).
- [13] M. Ippoliti and V. Khemani, Phys. Rev. Lett. 126, 060501 (2021).
- [14] M. Ippoliti, T. Rakovszky, and V. Khemani, Phys. Rev. X 12, 011045 (2022).
- [15] T.-C. Lu and T. Grover, PRX Quantum 2, 040319 (2021).
- [16] Y. Bao, S. Choi, and E. Altman, Phys. Rev. B 101, 104301 (2020).
- [17] G. Vidal and R. F. Werner, Phys. Rev. A 65, 032314 (2002).
- [18] M. B. Plenio, Phys. Rev. Lett. 95, 090503 (2005).
- [19] P. Calabrese, J. Cardy, and E. Tonni, Phys. Rev. Lett. 109, 130502 (2012).
- [20] P. Calabrese, J. Cardy, and E. Tonni, J. Stat. Mech. 02 (2013) P02008.
- [21] T.-C. Lu and T. Grover, Phys. Rev. B 99, 075157 (2019).
- [22] T.-C. Lu, T. H. Hsieh, and T. Grover, Phys. Rev. Lett. **125**, 116801 (2020).
- [23] K.-H. Wu, T.-C. Lu, C.-M. Chung, Y.-J. Kao, and T. Grover, Phys. Rev. Lett. 125, 140603 (2020).
- [24] T.-C. Lu and T. Grover, Phys. Rev. B **102**, 235110 (2020).
- [25] S. Sang, Y. Li, T. Zhou, X. Chen, T. H. Hsieh, and M. P. A. Fisher, PRX Quantum 2, 030313 (2021).
- [26] H. Shapourian, S. Liu, J. Kudler-Flam, and A. Vishwanath, PRX Quantum **2**, 030347 (2021).
- [27] P. Hayden, S. Nezami, X.-L. Qi, N. Thomas, M. Walter, and Z. Yang, J. High Energy Phys. 09 (2016) 11.
- [28] T. Zhou and A. Nahum, Phys. Rev. B 99, 174205 (2019).
- [29] C.-M. Jian, Y.-Z. You, R. Vasseur, and A. W. W. Ludwig, Phys. Rev. B 101, 104302 (2020).
- [30] X. Dong, X.-L. Qi, and M. Walter, J. High Energy Phys. 06 (2021) 024.
- [31] Y. Li, S. Vijay, and M. P. A. Fisher, arXiv:2105.13352.

- [32] M. Kardar, Phys. Rev. Lett. 55, 2923 (1985).
- [33] D. A. Huse, C. L. Henley, and D. S. Fisher, Phys. Rev. Lett. 55, 2924 (1985).
- [34] M. Kardar, G. Parisi, and Y.-C. Zhang, Phys. Rev. Lett. 56, 889 (1986).
- [35] M. Kardar, Statistical Physics of Fields (Cambridge University Press, Cambridge, New York, 2007).
- [36] U. Agrawal, A. Zabalo, K. Chen, J. H. Wilson, A. C. Potter, J. H. Pixley, S. Gopalakrishnan, and R. Vasseur, arXiv: 2107.10279.
- [37] M. A. Nielsen and I. L. Chuang, *Quantum Computation and Quantum Information*, 10th ed. (Cambridge University Press, Cambridge, New York, 2010).
- [38] D. A. Lidar, arXiv:1902.00967.
- [39] C. H. Bennett, D. P. DiVincenzo, J. A. Smolin, and W. K. Wootters, Phys. Rev. A 54, 3824 (1996).
- [40] M. Horodecki, P. Horodecki, and R. Horodecki, Phys. Rev. Lett. 80, 5239 (1998).
- [41] A. Peres, Phys. Rev. Lett. 77, 1413 (1996).
- [42] M. Horodecki, P. Horodecki, and R. Horodecki, Phys. Lett. A 223, 1 (1996).
- [43] G. Vidal and J. I. Cirac, Phys. Rev. Lett. **86**, 5803 (2001).
- [44] P. Horodecki, L. Rudnicki, and K. Zyczkowski, PRX Quantum 3, 010101 (2022).
- [45] D. Gottesman, arXiv:quant-ph/9807006.
- [46] S. Aaronson and D. Gottesman, Phys. Rev. A 70, 052328 (2004).
- [47] A. Hamma, R. Ionicioiu, and P. Zanardi, Phys. Lett. A 337, 22 (2005).
- [48] A. Hamma, R. Ionicioiu, and P. Zanardi, Phys. Rev. A 71, 022315 (2005).
- [49] See Supplemental Material at http://link.aps.org/supplemental/10.1103/PhysRevLett.129.080501 for a brief

- review of entanglement negativity as a mixed-state entanglement measure, details of our mixed-state stabilizer simulation, additional numerical results including finite-size scaling of the negativity and mutual information, and technical details of our statistical mechanics mapping.
- [50] Z. Webb, Quantum Inf. Comput. 16, 1379 (2016).
- [51] D. N. Page, Phys. Rev. Lett. 71, 1291 (1993).
- [52] U. T. Bhosale, S. Tomsovic, and A. Lakshminarayan, Phys. Rev. A 85, 062331 (2012).
- [53] A. Zabalo, M. J. Gullans, J. H. Wilson, S. Gopalakrishnan, D. A. Huse, and J. H. Pixley, Phys. Rev. B 101, 060301(R) (2020).
- [54] H. Nishimori, *Statistical Physics of Spin Glasses and Information Processing: An Introduction*, International Series of Monographs on Physics Vol. 111 (Oxford University Press, Oxford; New York, 2001).
- [55] B. Collins, Int. Math. Res. Not. 2003, 953 (2003).
- [56] B. Collins and P. Śniady, Commun. Math. Phys. 264, 773 (2006).
- [57] A. Nahum, S. Vijay, and J. Haah, Phys. Rev. X 8, 021014 (2018).
- [58] Y.-Z. You and Y. Gu, Phys. Rev. B 98, 014309 (2018).
- [59] In the zero temperature, late-time limit, we may assume that the polymer is "directed" in the *x* direction—that is, it has no loops or overhangs [35].
- [60] D. A. Huse and C. L. Henley, Phys. Rev. Lett. 54, 2708 (1985).
- [61] T. Gueudre and P. L. Doussal, Europhys. Lett. 100, 26006 (2012).
- [62] G. Barraquand, A. Krajenbrink, and P. Le Doussal, J. Stat. Phys. 181, 1149 (2020).
- [63] Z. Weinstein, Y. Bao, Z. Lenarčič, S. Choi, and E. Altman (to be published).
- [64] Y. Bao, S. Choi, and E. Altman, Ann. Phys. (Amsterdam) 435, 168618 (2021).